JAMES | Journal of Advances in Modeling Earth Systems

RESEARCH ARTICLE
10.1029/2020MS002190

Special Section:
The CNRM Climate and Earth System Models for CMIP6

Tracking Changes in Climate Sensitivity in CNRM Climate Models

D. Saint-Martin[1], O. Geoffroy[1], A. Voldoire[1], J. Cattiaux[1], F. Brient[2], F. Chauvin[1], M. Chevallier[1], J. Colin[1], B. Decharme[1], C. Delire[1], H. Douville[1], J.-F. Guérémy[1], E. Joetzjer[1], A. Ribes[1], R. Roehrig[1], L. Terray[3], and S. Valcke[3]

[1]CNRM, Université de Toulouse, CNRS, Toulouse, France, [2]LMD/IPSL, Sorbonne Université, Paris, France, [3]CECI, Université de Toulouse, CNRS, CERFACS, Toulouse, France

Key Points:

- The CNRM climate models contributing to Coupled Model Intercomparison Project phase 6 have a larger climate sensitivity than their CMIP5 predecessor
- The climate sensitivity increase is the result of changes in the atmospheric component, through the dominant role of tropical cloud changes
- The new convection scheme appears to play an important role in driving the cloud changes

Supporting Information:

Supporting Information may be found in the online version of this article.

Correspondence to:

D. Saint-Martin,
david.saint-martin@meteo.fr

Citation:

Saint-Martin, D., Geoffroy, O., Voldoire, A., Cattiaux, J., Brient, F., Chauvin, F., et al. (2021). Tracking changes in climate sensitivity in CNRM climate models. *Journal of Advances in Modeling Earth Systems*, *13*, e2020MS002190. https://doi.org/10.1029/2020MS002190

Received 12 JUN 2020
Accepted 10 DEC 2020

Abstract The equilibrium climate sensitivity (ECS) in the latest version of CNRM climate model, CNRM-CM6-1, and in its high-resolution counterpart, CNRM-CM6-1-HR, is significantly larger than in the previous version (CNRM-CM5.1). The traceability of this climate sensitivity change is investigated using coupled ocean-atmosphere model climate change simulations. These simulations show that the increase in ECS is the result of changes in the atmospheric component. A particular attention is paid to the method used to decompose the equilibrium temperature response difference, by using a linearized decomposition of the individual radiative agents diagnosed by a radiative kernel technique. The climate sensitivity increase is primarily due to the cloud radiative responses, with a predominant contribution of the tropical longwave response (including both feedback and forcing adjustment) and a significant contribution of the extratropical and tropical shortwave feedback changes. A series of stand-alone atmosphere experiments is carried out to quantify the contributions of each atmospheric development to this difference between CNRM-CM5.1 and CNRM-CM6-1. The change of the convection scheme appears to play an important role in driving the cloud changes, with a large effect on the tropical longwave cloud feedback change.

Plain Language Summary The global equilibrium temperature change in response to a doubling of the atmospheric carbon dioxide concentration is an important characteristic of the climate system known as the equilibrium climate sensitivity (ECS). Many climate models contributing to CMIP6 (Coupled Model Intercomparison Project phase 6) have a larger ECS than their CMIP5 predecessors. Here, we investigate the origins of this increase for the CNRM model and its high-resolution version. We find that it primarily results from changes in the atmospheric component, in particular in the convection scheme, through its impact on the cloud radiative responses.

1. Introduction

The global temperature changes in response to an externally imposed radiative perturbation or climate sensitivity is an important feature of the climate system. It is often quantified by the equilibrium climate sensitivity (ECS), that is, the stationary-state global-mean surface-air temperature change in response to a doubling of the atmospheric carbon dioxide (CO_2) concentration. The spread in climate model ECS (Flato et al., 2013; Meehl et al., 2007) has remained large throughout the successive phases of the Coupled Model Intercomparison Project (CMIP5; Taylor et al. (2012); CMIP6; Eyring et al. [2016]). The identification of the key mechanisms responsible for this spread and the quantification of their contributions is a necessary step to better understand climate change.

The surface temperature response to a radiative forcing causes radiative feedbacks within the system that can amplify or dampen the temperature response (e.g., Hansen et al., 1984; Wetherald & Manabe, 1988). In particular, these radiative agents include air temperature, water vapor, surface albedo, and clouds (e.g., Soden & Held, 2006). They can also change at fast time scales, adding a fast adjustment component to the instantaneous radiative forcing (J. Gregory & Webb, 2008). A commonly used method to decompose the effect of each radiative agent consists in using radiative kernels (Shell et al., 2008; Soden & Held, 2006). Using this technique, the climate sensitivity can be broken down into the sum of the different contributions associated with each radiative agent. The method used for the decomposition can significantly impact the

results (Caldwell et al., 2016). Finally, when using fixed sea surface temperature (SST) experiments to compute these values, the choice of the SST field can also be important due to the so-called pattern effect, that is, the sensitivity of the feedbacks to the ocean surface warming pattern (Winton et al., 2010).

The intermodel differences in both the radiative feedbacks and the forcing adjustments are important sources of spread for climate sensitivity (e.g., Geoffroy et al., 2012). Clouds, in particular low level clouds, have been identified as the most uncertain feedbacks of the climate system (Bony & Dufresne, 2005; Bony et al., 2006; Cess et al., 1990; Soden & Held, 2006; Vial et al., 2013; Zelinka et al., 2013). Atmospheric parameterizations constitute the main source of these differences in the climate model responses (e.g., Medeiros et al., 2008; Ringer et al., 2014). In particular the representation of convection including convective microphysics is likely to be the most uncertain process, as shown by perturbed physics ensemble studies (Collins et al., 2010; Tomassini et al., 2015; Zhao et al., 2016) and diagnostic studies (Sherwood et al., 2014). Other schemes have also been suggested to play a substantial role such as large-scale microphysics, turbulence, or cloud schemes (Bodas-Salcedo et al., 2019; Geoffroy et al., 2017; Qu et al., 2014; Tan et al., 2016).

The climate sensitivity of the CMIP6 version of CNRM-CM has drastically increased compared to its previous CMIP5 version (Voldoire et al., 2019). Recently, Zelinka et al. (2020) have shown that the ECS has increased substantially in CMIP6 models. They argue that this increase is mainly due to a stronger positive cloud feedback associated with a decrease in extratropical low cloud coverage and albedo. This behavior concerns the multimodel mean but large differences across climate models remain.

As recently done by Gettelman et al. (2019) for the Community Earth System Model Version 2 (CESM2) or by Bodas-Salcedo et al. (2019) for the Hadley Centre Global Environmental model (HadGEM3), here we document the ECS changes in the CNRM suite of climate models: from the CMIP5 version CNRM-CM5.1 (Voldoire et al., 2013) to the CMIP6 versions, CNRM-CM6-1 (Voldoire et al., 2019) and its high-resolution counterpart CNRM-CM6-1-HR. To this aim, we have performed intermediate configuration experiments to disentangle the contribution of each component to the ECS change. For each of these configurations, we decompose the ECS change in each radiative agent contribution through radiative kernels. A particular care is paid to the method used to decompose the equilibrium temperature response difference. The coupled atmosphere-ocean general circulation models (AOGCM) of the CNRM suite are briefly summarized in Section 2. The experimental setup is described in Section 3, while Section 4 details the methodology used to derive the forcing and the feedback parameters and the new decomposition method proposed to separate the contributions from the different radiative agents when differentiating model versions. Results are presented in Section 5.

2. Description of the CNRM-CM Climate Models

2.1. CNRM-CM6-1 (CM6)

CNRM-CM6-1 (hereafter CM6) is the CNRM-CM climate model developed in the context of CMIP6 (Eyring et al., 2016). It is based on ARPEGE-Climat v6.3 for the atmosphere, NEMO v3.6 for the ocean (Madec et al., 2017), SURFEX v8.0 for the land surface coupled to CTRIP v2 for the river routing (Decharme et al., 2019), and GELATO v6 for the sea-ice, these components being coupled via the OASIS3-MCT software (Craig et al., 2017). The atmospheric horizontal resolution is 140 km and there are 91 atmospheric layers (up to 0.01 hPa), while the oceanic resolution is 1° with a latitudinal refinement to 1/3° at the Equator and 75 vertical levels. A complete description and validation of this model is provided in Voldoire et al. (2019).

2.2. CNRM-CM6-1-HR (CM6-HR)

This model is the high-resolution version of CNRM-CM6-1 (hereafter CM6-HR). It is based on the same components and the only difference is the increase in horizontal resolution from 140 to 50 km in the atmosphere and from 1° to 0.25° in the ocean, the vertical resolutions being unchanged. Along with the increased ocean horizontal resolution, a few ocean parameters have been adapted. The time step is reduced from 30 to 15 min, the lateral diffusion is reduced as some eddies are represented at this resolution and the Gent and McWilliams parameterization (Gent & McWilliams, 1990) of eddies is switched off. The tidal mixing scheme is changed to the one based on Simmons et al. (2004), which is more stable at 0.25° resolution than

Table 1
Atmospheric Parameterizations of CNRM-CM5.1 and CNRM-CM6-1 Models Grouped Into Five Main Packages

	CNRM-CM5.1	CNRM-CM6-1
Vertical resolution dynamics	31 layers (TOA: 10 hPa)	91 layers (TOA: 0.01 hPa)
Microphysics	Kessler (1969) R. N. Smith (1990)	Lopez (2002)
Turbulence large-scale clouds	Mellor & Yamada (1982) Bougeault (1981) Bougeault (1982) Ricard & Royer (1993)	Bougeault & Lacarrère (1989) Cuxart et al. (2000) Cheng et al. (2002) Ricard & Royer (1993)
Convection	Bougeault (1985)	Piriou et al. (2007) Guérémy (2011)
Cloud optical properties	Slingo (1988) Ebert & Curry (1992) E. A. Smith & Shi (1992)	Slingo (1988) Fu (1996) E. A. Smith & Shi (1992)

the recently developed scheme of de Lavergne et al. (2015) activated in CNRM-CM6-1. For all other components (atmosphere, land surface, and sea-ice), there has been no additional tuning. Thus, CNRM-CM6-1-HR model can be considered as a higher-resolution version of CNRM-CM6-1. Climatologies of surface temperature and precipitation in CNRM-CM6-1-HR and CNRM-CM6-1 are evaluated and compared in Figures S1 and S2. The climate mean states of the two models are rather similar.

2.3. CNRM-CM5.1 (CM5)

CNRM-CM5.1 (hereafter CM5) was developed for the former CMIP phase (CMIP5; Taylor et al., 2012). It is based on older versions of the CM6 components. The reader is referred to Voldoire et al. (2013) for a full description and to Voldoire et al. (2019) for a detailed description of the differences with regards to CM6. Aside from bugfixes and code optimization, the main elements that will be of importance for this study are the change in vertical resolution (42 oceanic layers and 31 atmospheric layers up to 10 hPa in CM5); and the change of the complete set of atmospheric parameterizations (mainly convection, turbulence, and microphysics). Differences between atmospheric parameterizations are summarized in Table 1.

2.4. CNRM-CM6-atm5 (CM6-atm5)

In this configuration, we replaced the atmospheric component of CM6 by one of the CM5. Only slight adjustments in the aerosol and cloud optical properties have been done to tune the radiative imbalance of the climate system.

3. Experimental Setup

For each CNRM-CM coupled AOGCM, the climate sensitivity is evaluated by using the abrupt-4×CO_2 experiments in which the atmospheric CO_2 concentration is abruptly quadrupled. For CM5, CM6, and CM6-HR, data are available in the CMIP5 and CMIP6 databases. For the intermediate configuration, CM6-atm5, similar experiments were carried out. The changes in abrupt-4×CO_2 experiments are evaluated against 500-year time averages of the piControl experiment and denoted by the Δ operator.

To investigate the role of the atmospheric components in the climate sensitivity change from CM6-atm5 to CM6, we use fixed-SST experiments. The set of atmosphere-only experiments corresponding to CM6-atm5 (respectively CM6) is denoted by AM5 (respectively AM6). These atmosphere-only runs are computationally less expensive than AOGCM experiments and allow to test the effects of multiple changes to the atmospheric model suite. Experiments such as +4 K uniform warming experiments (Cess et al., 1990) have been widely used to asses models climate sensitivity (e.g., Gettelman et al., 2012). Indeed, the estimates of climate sensitivity from fixed-SST experiments are consistent with those determined from coupled atmosphere-ocean simulations (e.g., Ringer et al., 2014). However, they cannot be fully identical due to the pattern effect (e.g., Winton et al., 2010). Here, we use monthly mean SST and sea-ice cover (SIC) derived from their respective coupled AOGCM piControl and abrupt4×CO_2 simulations so that atmospheric changes in coupled and fixed-SST experiments are in very close agreement (Andrews et al., 2015).

Table 2
List of Fixed-SST Experiments

Experiment name	$[CO_2]$	Prescribed SST/SIC
piSST_piCO$_2$	$[CO_2]_{pi}$	Clim. of 500 years of the piControl experiment
piSST_4×CO$_2$	$4[CO_2]_{pi}$	Clim. of 500 years of the piControl experiment
4 × SST_4 ×CO$_2$	$4[CO_2]_{pi}$	Clim. of last 30 years (years 121–150) of the abrupt-4×CO$_2$ experiment

Note. Specification of the CO_2 forcing and prescribed SST/SIC. $[CO_2]_{pi}$ corresponds to the preindustrial value of atmospheric CO_2 concentration.

We use three types of atmosphere-only experiments (see Table 2). The first one uses climatological SST/SICs derived from the 500-year period of the piControl experiment and preindustrial values for the CO_2 concentration: piSST_piCO$_2$. In the second one (piSST_4×CO$_2$), the prescribed SST/SICs are identical to the first experiment but the CO_2 concentration is abruptly quadrupled and maintained fixed. In the third one (4×SST_4×CO$_2$), the CO_2 concentration is 4 times the preindustrial values and the prescribed SST/SICs are derived from the multiyear climatology of the last 30 years (years 121–150) of the corresponding abrupt-4×CO$_2$ experiment. Each experiment is 10-year long. The temporal mean of each experiment is used and differences between piSST_4×CO$_2$ and piSST_piCO$_2$, and between 4×SST_4×CO$_2$ and piSST_piCO$_2$ are denoted by Δ_{pi} and $\Delta_{4\times}$, respectively.

To investigate the impact of the SST differences on the forcing adjustment and the radiative feedbacks, we perform the fixed-SST experiments in the AM5 configuration but with the monthly climatology of SST/SIC derived from the CM6 AOGCM experiments. This configuration is named AM5-s6. Differences between AM5 and AM5-s6 can arise from differences in the mean value and the geographical pattern of the prescribed SST field. This effect is referred to as "SST effect."

We also carry out a series of modifications that sequentially replace AM5 modules or options until the final atmospheric model is identical to AM6 (cf. Tables 1 and 3). The series of changes are determined by the model structure and dependencies. As noted in Table 3, we first modify the vertical resolution and associated dynamical options and physical parameterizations. Then, we sequentially replace the cloud microphysics, the turbulence, and large-scale cloud schemes, the convection scheme and finally the clouds and aerosols radiative properties.

Table 3
List of Fixed-SST Experiments

Experiment name	SST	Vert. Res./dyn.	Microphysics	Turb./cloud	Convection	Radiation
AM5	CM6-atm5	atm5	atm5	atm5	atm5	atm5
AM5-s6	CM6	atm5	atm5	atm5	atm5	atm5
AM5-d6	CM6	atm6	atm5	atm5	atm5	atm5
AM5-m6	CM6	atm6	atm6	atm5	atm5	atm5
AM5-t6	CM6	atm6	atm6	atm6	atm5	atm5
AM5-c6	CM6	atm6	atm6	atm6	atm6	atm5
AM6	CM6	atm6	atm6	atm6	atm6	atm6

Note. AM5 experiment corresponds to the atmospheric component of CM6-atm5 model and uses prescribed SST/SIC from CM6-atm5 piControl and abrupt-4×CO$_2$ experiments. AM5-s6 corresponds to the atmospheric component of CM6-atm5 model and uses prescribed SST/SIC from CM6 piControl and abrupt-4×CO$_2$ experiments. AM6 experiment corresponds to the atmospheric component of CM6 model and uses prescribed SST/SIC from CM6 piControl and abrupt-4×CO$_2$ experiments. From AM5-s6 experiment to AM6 experiment, changes correspond to changes in atmospheric model and are grouped into five packages: Vertical resolution and dynamics, microphysics, turbulence and clouds, convection and radiation. Specifications associated with each package are described in Table 1.

4. Methodology

4.1. Equilibrium Temperature Response

The $4\times CO_2$ equilibrium temperature response (referred to as ΔT_{eq}) is estimated by linear regression of the annual-mean global-mean net radiative TOA response ΔR against the annual-mean global-mean surface-air temperature response ΔT_s during the first 150 years in the abrupt-$4\times CO_2$ experiment (J. M. Gregory et al., 2004):

$$\Delta R = F_{tot} + \lambda_{tot}\Delta T_s \text{ and } \Delta T_{eq} = -\frac{F_{tot}}{\lambda_{tot}} \tag{1}$$

where F_{tot} is the stratosphere-troposphere adjusted global radiative forcing and λ_{tot} is the total feedback parameter. ΔT_{eq} is often scaled by a factor of 0.5 to obtain ECS by assuming a log-linear CO_2-forcing relationship. Because the CO_2 forcing rises slightly faster than logarithmic (Etminan et al., 2016) and because the climate feedbacks may vary with the equilibrium climate state (Geoffroy & Saint-Martin, 2020; J. M. Gregory et al., 2015), we focus on the change in ΔT_{eq} without any rescaling. As in Andrews et al. (2012), we construct 95% confidence intervals associated with our estimates of F_{tot}, λ_{tot}, and ΔT_{eq} using a bootstrap method. Random samples (with replacement) of 150 years are used to produce a probability density function of the required values.

In atmosphere-only experiments, due to the temperature change over land in the piSST_$4\times CO_2$ experiment, the radiative imbalance $\Delta_{\text{pi}}R$ is not equal to the stratosphere-troposphere adjusted global radiative forcing F_{tot}. It is referred to as $F^*_{tot} = \Delta_{\text{pi}}R$. F^*_{tot} also includes the radiative response associated with the land temperature adjustment $\Delta T_L = \Delta_{\text{pi}}T_s$. The feedback parameter λ_{tot} can be estimated as:

$$\lambda_{tot} = \frac{\Delta_{4\text{x}}R - \Delta_{\text{pi}}R}{\Delta_{4\text{x}}T_s - \Delta_{\text{pi}}T_s}, \tag{2}$$

with $\Delta_{\text{pi}}X = X_{\text{piSST}_{4\text{x}}\text{CO}_2} - X_{\text{piSST}_{\text{pi}}\text{CO}_2}$ and $\Delta_{4\text{x}}X = X_{4\text{xSST}_{4\text{x}}\text{CO}_2} - X_{\text{piSST}_{\text{pi}}\text{CO}_2}$. The equilibrium temperature response ΔT_{eq} writes:

$$\Delta T_{eq} = -\frac{F_{tot}}{\lambda_{tot}} = \Delta T_L - \frac{F^*_{tot}}{\lambda_{tot}}. \tag{3}$$

4.2. Radiative Kernels

The net radiative flux at TOA can be written as a function of the atmospheric CO_2 concentration c, of the global near surface-air temperature T_s, and of atmospheric radiative agents x_i (air temperature, specific humidity, surface albedo, and clouds): $R \equiv R(c, T_s, x_i(c, T_s))$. A perturbation of this radiative flux, small enough to allow linearization, can be written as (Geoffroy et al., 2014; Wetherald & Manabe, 1988):

$$\Delta R = \frac{\partial R}{\partial c}\Delta c + \sum_i \left(\frac{\partial R}{\partial x_i}\frac{\partial x_i}{\partial c}\Delta c + \frac{\partial R}{\partial x_i}\frac{\partial x_i}{\partial T_s}\Delta T_s \right) + \Delta R_r. \tag{4}$$

The forcing adjustment associated with each field i is defined as: $F_i = (\partial_{x_i}R)(\partial_c x_i)\Delta c$. The global forcing ($F_{\text{tot}}$) is the sum of the stratosphere-adjusted forcing $\mathcal{F}_0 = (\partial_c R)\Delta c$ and the individual contributions to the forcing adjustment, $F_{tot} = \mathcal{F}_0 + \sum_i F_i$. The feedback parameter λ_i associated with each field i is defined as: $\lambda_i = (\partial_{x_i}R)(\partial_{T_s}x_i)$. $\Delta R_r \equiv \lambda_r \Delta T_s$ is a residual term, resulting from linearization. The total radiative feedback parameter (λ_{tot}) is the sum of the individual feedback and of the residual feedback, $\lambda_{\text{tot}} = \sum_i \lambda_i + \lambda_r$.

The individual feedback parameters and adjustment forcings are estimated using the radiative kernel technique (Soden & Held, 2006; Soden et al., 2008). The linear response function, $K_i = \partial_{x_i}R$, that is, the change in TOA fluxes due to a standard change in a physical climate variable (x_i) is called the radiative kernel. Kernels are calculated using a radiative transfer model. They depend on the radiative transfer code and on the control state of the atmosphere (e.g., Block & Mauritsen, 2013; Tomassini et al., 2013). To ensure consistency between the kernel computations and the analyzed model (and in order to quantify uncertainties

relative to the use of different kernels) we use the radiative kernels derived from CNRM-CM radiative transfer model with cloud and aerosol optical properties from CM6-atm5 model and CM6 model. To facilitate comparison with previous studies, we also computed contributions from the radiative kernels of the Community Atmospheric Model version 3 (CAM3; Shell et al., 2008).

The individual feedbacks are estimated from the piSST_4×CO_2 and 4×SST_4×CO_2 experiments:

$$\lambda_i = K_i \frac{\Delta_{4x} x_i - \Delta_{pi} x_i}{\Delta_{4x} T_s - \Delta_{pi} T_s}. \tag{5}$$

When differentiating piSST_4×CO_2 and piSST_piCO_2, we obtain $F^*_{tot} = \Delta_{pi} R = \mathcal{F}_0 + \sum_i K_i \Delta_{pi} x_i$. The contributions $F^*_i = K_i \Delta_{pi} x_i$ are not exactly equal to the individual forcing adjustment contributions, F_i. They correspond to the tropospheric adjustments to CO_2 forcing and they also include the radiative response associated with the land surface warming adjustment. The land temperature fast adjustment is not broken into different feedback contributions and remains as an additional term in the equilibrium temperature change decomposition. Finally, by expanding Equation 3, the decomposition of the equilibrium temperature response writes:

$$\Delta T_{eq} = \Delta_{pi} T_s - \frac{\mathcal{F}_0 + \sum_i F^*_i}{\sum_i \lambda_i + \lambda_r}. \tag{6}$$

We compute radiative kernels for air temperature, water vapor, and surface albedo. The temperature feedback is split into Planck feedback and lapse rate feedback. The cloud feedbacks are estimated by using a decomposition of the difference in radiative imbalance in all-sky and clear-sky conditions (Soden et al., 2008).

4.3. ECS Decomposition

Once we have decomposed the change in total forcing adjustment and feedback parameter (Equation 6), we are interested in quantifying the contribution of these forcing and feedback terms to the climate sensitivity difference between two model configurations (denoted by a and b). The change between $-F_a/\lambda_a$ (with $F_a = \sum_i F_{a,i}$ and $\lambda_a = \sum_j \lambda_{a,j}$) and $-F_b/\lambda_b$ (with $F_b = \sum_i F_{b,i}$ and $\lambda_b = \sum_j \lambda_{b,j}$) can be written as the sum of individual contribution of the ith forcing, $\Delta_{ab} T_{F_i}$, of the jth feedback, $\Delta_{ab} T_{\lambda_j}$ and a residual term accounting for interactions:

$$-\frac{F_b}{\lambda_b} + \frac{F_a}{\lambda_a} = \sum_i \Delta_{ab} T_{F_i} + \sum_j \Delta_{ab} T_{\lambda_j} + \Delta_{ab} T_R. \tag{7}$$

This decomposition has been used previously in Caldwell et al. (2016) and simply results from the linearization of the function, E: $(\mathbf{F}, \boldsymbol{\lambda}) \mapsto \mathbf{F}/\boldsymbol{\lambda}$. $\Delta_{ab} T_{F_i} = (\partial_{F_i} E) \Delta_{ab} F_i$ and $\Delta_{ab} T_{\lambda_j} = (\partial_{\lambda_j} E) \Delta_{ab} \lambda_j$. The residual term of this linearization ($\Delta_{ab} T_R$) is significant if $\Delta_{ab} \lambda_j$ or $\Delta_{ab} F_i$ are quite large. To estimate the partial derivatives of E, we choose to average the values at ($\mathbf{F}_a$, $\boldsymbol{\lambda}_a$) and ($\mathbf{F}_b$, $\boldsymbol{\lambda}_b$). Finally, we have:

$$\Delta_{ab} T_{F_i} = -\frac{1}{2}\left(\frac{1}{\lambda_a} + \frac{1}{\lambda_b}\right)(F_{b,i} - F_{a,i}), \tag{8}$$

$$\Delta_{ab} T_{\lambda_j} = \frac{1}{2}\left(\frac{F_a}{\lambda_a^2} + \frac{F_b}{\lambda_b^2}\right)(\lambda_{b,j} - \lambda_{a,j}). \tag{9}$$

By using Equation 6, the complete decomposition of the change in the equilibrium temperature response writes:

$$\Delta_{ab} T_{eq} = \Delta_{ab} T_L + \Delta_{ab} T_{F^*} + \Delta_{ab} T_\lambda + \Delta_{ab} T_R \tag{10}$$

where $\Delta_{ab} T_{eq} = \Delta T_{eq,b} - \Delta T_{eq,a}$, $\Delta_{ab} T_L = \Delta T_{L,b} - \Delta T_{L,a}$ is the contribution from the change in land surface warming adjustment, $\Delta_{ab} T_{F^*} = \sum_i \Delta_{ab} T_{F_i^*}$ is the sum of the individual contributions of forcing adjustment change, and $\Delta_{ab} T_\lambda = \sum_j \Delta_{ab} T_{\lambda_j}$ is the sum of the individual contributions of feedback change.

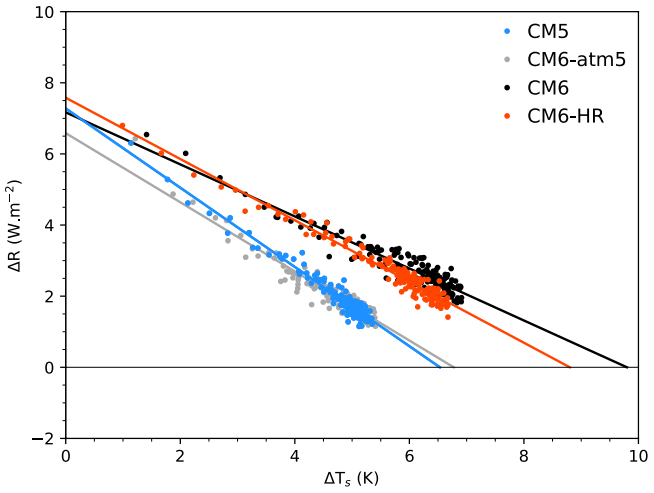

Figure 1. Scatterplot of the global-mean surface-air temperature response (ΔT_s, unit: K) and net TOA radiative imbalance (ΔR, unit: W.m^{-2}) in the CNRM-CM abrupt-4×CO_2 experiments: CNRM-CM5 (blue), CNRM-CM6-atm5 (gray), CNRM-CM6-1 (black), and CNRM-CM6-1-HR (red).

This linearized method is preferred to the decomposition described in Dufresne and Bony (2008, hereafter DB08). Details of the derivation of the DB08 decomposition are presented in Appendix A. As previously noted by Caldwell et al. (2016), the DB08 decomposition can lead to erroneous interpretation when quantifying the role of each individual radiative agent in the climate sensitivity difference between two model configurations. In particular, the contribution of an individual feedback change $\Delta_{ab}T_{\lambda_i}$ could be nonzero even if $\lambda_{a,i}$ and $\lambda_{b,i}$ are equal.

5. Results

5.1. Role of the Atmosphere

Figure 1 shows the scatter plot of the joint temporal evolution of the annual-mean global-mean surface-air temperature response ΔT_s and the net radiative TOA response ΔR for each CNRM-CM configuration. The values of the stratosphere-troposphere adjusted global radiative forcing F_{tot} and the total feedback parameter λ_{tot} are estimated by linear regression (J. M. Gregory et al., 2004) and are summarized in Table 4.

The CM6-HR and CM6 configurations show relatively similar responses to a quadrupling of CO_2, with equilibrium temperature response of 8.8 and 9.8 K. The change in atmospheric and oceanic horizontal resolutions has a small effect on the model response, consistent with the small dependence of climate sensitivity to horizontal resolution in the CMIP5 ensemble (e.g., Table 9.5 in Flato et al. [2013]). Further investigation of this difference would have required additional experiments that were unaffordable due to the computational cost of this version. In the following, we rather focus on explaining the difference with the former version which is 3 times larger in magnitude.

The modification of the evapotranspiration effect (Keenan et al., 2013) through the parameterization of the CO_2-induced stomatal closure process in CNRM-CM6-1 has also little impact on the radiative response to a CO_2 perturbation (see Table 4).

On the contrary, the 4×CO_2 equilibrium temperature response of CM6 (9.8 K) is significantly larger than that of the previous version CM5 (6.4 K). All components of the climate system, the atmosphere, the land, the cryosphere and the ocean, differ between the two versions. The CM6-atm5 configuration has a 4×CO_2 equilibrium temperature response of 6.8 K showing that the change of climate sensitivity from CMIP5 model to CMIP6 models can essentially be attributed to the change in the atmospheric component. In the next section, we investigate the atmospheric source of the climate sensitivity change from CM6-atm5 to CM6.

Table 4
Values of Troposphere-Stratosphere Adjusted Radiative Forcing F_{tot}, Total Radiative Feedback Parameter λ_{tot}, and Equilibrium Temperature Response ΔT_{eq} Estimated by Linear Regression During the First 150 Years in the abrupt-4 × CO_2 Experiment (J. M. Gregory et al., 2004)

Configuration	F_{tot} (W.m^{-2})	λ_{tot} (W.m^{-2}.K^{-1})	ΔT_{eq} (K)
CM5	7.28 [7.01, 7.53]	−1.11 [−1.16, −1.06]	6.53 [6.45, 6.62]
CM6-atm5	6.58 [6.07, 6.99]	−0.97 [−0.87, −1.06]	6.77 [6.62, 6.94]
CM6-evaptr	6.85 [6.47, 7.09]	−0.69 [−0.73,−0.63]	9.90 [9.68, 10.28]
CM6	7.17 [6.83, 7.41]	−0.73 [−0.77, −0.67]	9.80 [9.60, 10.11]
CM6-HR	7.58 [7.40, 7.80]	−0.86 [−0.90, −0.83]	8.80 [8.67, 8.93]

Note. Values in brackets correspond to 95% confidence interval (see Section 4.1).

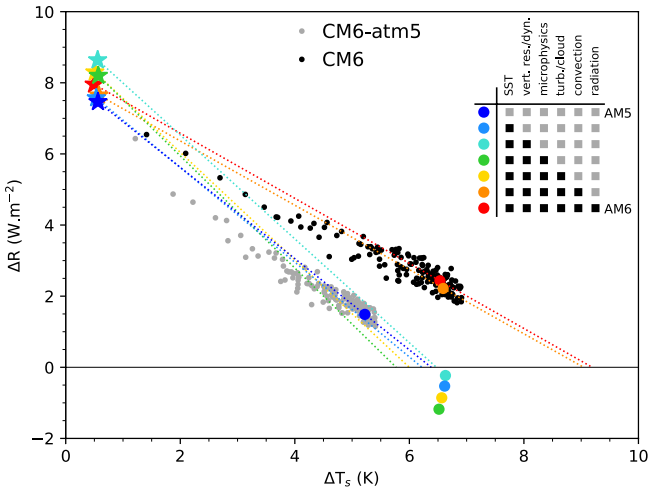

Figure 2. Scatterplot of the global-mean surface-air temperature response (ΔT_s, unit: K) and net TOA radiative imbalance (ΔR, unit: W.m^{-2}) in the CM6-atm5 (gray) and CM6 (black) abrupt-4×CO_2 experiments. Colored stars correspond to ($\Delta_{pi}T_s$, $\Delta_{pi}R$) and colored circle correspond to ($\Delta_{4\times}T_s$, $\Delta_{4\times}R$) for each fixed-SST experiments. Sequential changes in fixed-SST experiments are summarized in Table 3.

5.2. Individual Contributions of Atmospheric Components

Figure 2 reproduces the joint temporal evolution of the annual-mean global-mean surface-air temperature response ΔT_s and the net radiative TOA response ΔR in the abrupt-4×CO_2 experiments carried out with CM6 (black dots) and CM6-atm5 (gray dots). The values of ($\Delta_{pi}T_s$, $\Delta_{pi}R$) (stars) and ($\Delta_{4\times}T$, $\Delta_{4\times}R$) (circles) are superimposed for the fixed-SST experiment AM5 (blue star and circle) and AM6 (red star and circle) with the SST/SIC climatologies from their respective coupled AOGCM simulations (see Table 3). Note that, as identical SST/SICs are prescribed in piSST_piCO_2 and piSST_4×CO_2 experiments, the temperature change $\Delta_{pi}T_s$ is only due to the land warming. The fixed-SST experiments reproduce very well the beginning and the end of the radiative response simulated by the AOGCM (blue and red circles are in the neighborhood of the corresponding gray and black dots).

The 4×CO_2 equilibrium temperature response of AM5 and AM6 calculated from Equation 3 are given in Table 5. Their difference is 2.81 K. Note that this estimate slightly differs from the difference in equilibrium temperature response between CM6 and CM6-atm5 obtained by linear regression of the abrupt-4×CO_2 experiment (3.0 K) due to equilibrium- and transient-state dependencies of the climate feedbacks (e.g., Geoffroy & Saint-Martin, 2020). When removing the SST effect (AM5-s6 differs from AM5 in the mean value and the geographical pattern of the prescribed SST field), the difference in 4×CO_2 equilibrium temperature response between AM5-s6 and AM6 is equal to 3.0 K, close to the difference between the coupled CM6 and CM6-atm5.

We sequentially replace AM5 modules or options until the final atmospheric model is identical to AM6 (see Section 3). The values of ($\Delta_{pi}T_s$, $\Delta_{pi}R$) and ($\Delta_{4\times}T$, $\Delta_{4\times}R$) corresponding to this series of modifications are plotted in Figure 2 and summarized in Table 5 for each intermediate configuration. Changing vertical resolution, cloud microphysics, and turbulence/cloud schemes has limited effects on equilibrium temperature response. The individual effects are of order of 0.20 K, with a maximum effect of −0.70 K for microphysics. The final modification of cloud and aerosol properties also very slightly changed ΔT_{eq}. Thus, the main contributor to the climate sensitivity difference between AM5 and AM6 is the change of the convection scheme.

In the next section, the change in climate sensitivity is decomposed into contributions of both F^*_{tot} and λ_{tot} (see Equation 3) associated with change in the different radiative agents.

Table 5
Estimates of the Troposphere-Stratosphere Adjusted Radiative Forcing F_{tot}, of the Total Radiative Feedback Parameter λ_{tot}, and of the Equilibrium Temperature Response ΔT_{eq} in Fixed-SST Experiments

Experiment name	F_{tot} (W.m^{-2})	λ_{tot} (W.m^{-2}.K^{-1})	ΔT_{eq} (K)
AM5	8.19	−1.28	6.38
AM5-s6	8.28	−1.33	6.22
AM5-d6	9.45	−1.46	6.47
AM5-m6	9.10	−1.58	5.77
AM5-t6	9.07	−1.51	6.00
AM5-c6	8.17	−0.90	9.04
AM6	8.41	−0.91	9.19

Note. $F_{tot} = \Delta_{pi}R - \lambda_{tot}\Delta_{pi}T_s$ and $\lambda_{tot} = (\Delta_{4\times}R - \Delta_{pi}R)/(\Delta_{4\times}T_s - \Delta_{pi}T_s)$

5.3. Role of the Different Radiative Agents in Climate Sensitivity Change

The climate sensitivity decomposition method described in Section 4.3 is used jointly to the kernel radiative decomposition method. Global-mean values of individual radiative feedback (λ_i) and forcing adjustment (F^*_i) for each fixed-SST experiment and for each radiative kernel are available in supporting information (Tables S2–S5).

First, the decomposition of the change in the 4×CO_2 equilibrium temperature response (Equations 7 and 10) is applied to the change between AM5 and AM6 experiments ($\Delta_{ab}T_{eq}$ = 2.81 K). This linearized decomposition is summarized in three ways in Figure 3a: the first one (gray bars on the left part of Figure 3a) to disentangle the role of total forcing adjustment, total feedback, and land warming adjustment, the second one (colored bars on the middle of Figure 3a) to derive the relative role of each radiative agents—Planck, lapse rate and water vapor, albedo, shortwave and longwave clouds—and the third one (gray bars with colored

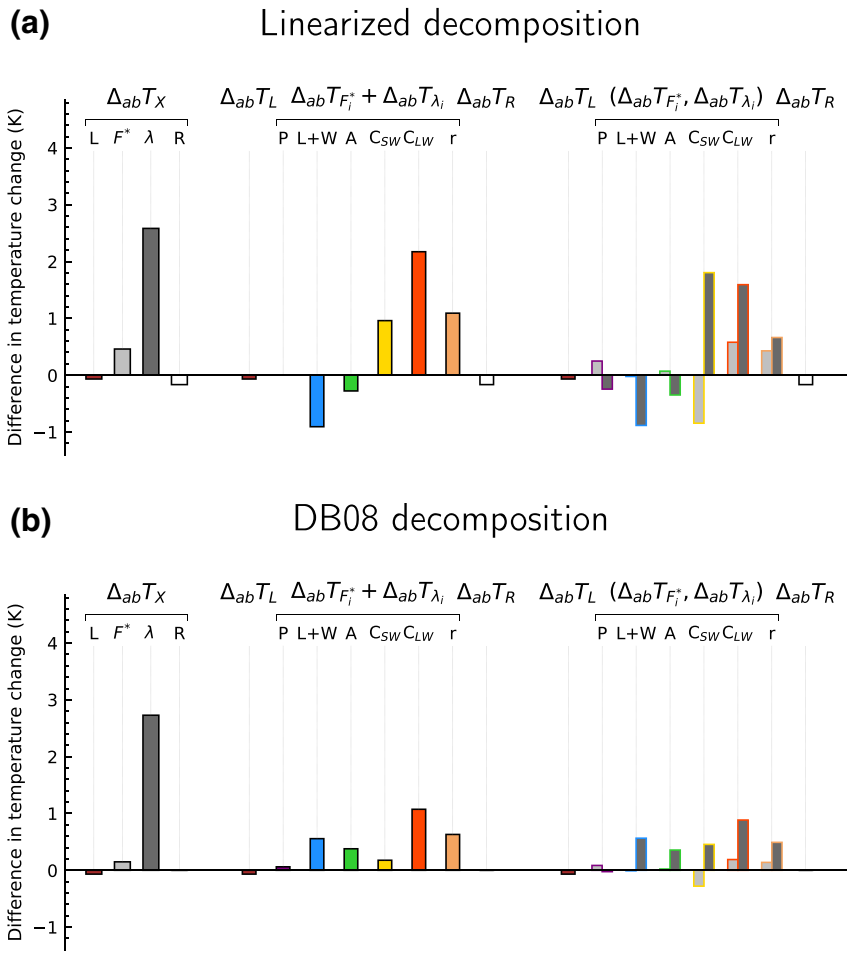

Figure 3. Decomposition of the difference in 4×CO_2 equilibrium temperature response between AM5 and AM6, for (a) the linearized decomposition presented in Section 4.3 and (b) the DB08 decomposition described in Dufresne and Bony (2008). In each panel, the difference in equilibrium temperature response between model configurations *a* (AM5) and *b* (AM6), $\Delta_{ab}T_{\mathrm{eq}}$ (black), is decomposed 3 times: (left part) into the land warming adjustment contribution $\Delta_{ab}T_L$ (brown), the forcing adjustment contribution $\Delta_{ab}T_{F^*}$ (light gray), the feedback contribution $\Delta_{ab}T_\lambda$ (gray), and the residual term $\Delta_{ab}T_R$ (white), (middle part) into the individual radiative agents contribution $\Delta_{ab}T_{F_i^*} + \Delta_{ab}T_{\lambda_i}$ (colored), the land warming adjustment contribution $\Delta_{ab}T_L$ (brown) and the residual term $\Delta_{ab}T_R$ (white) and (right part) into the individual radiative agents contributions of forcing adjustment change $\Delta_{ab}T_{F_i^*}$ (light gray with colored edges), the individual contributions of feedback change $\Delta_{ab}T_{\lambda_i}$ (gray with colored edges) and into the land warming adjustment contribution $\Delta_{ab}T_L$ (brown) and the residual term. Radiative agents are the Planck feedback (P), the lapse rate and water vapor feedback (L + W), the albedo feedback (A), the cloud feedback on solar radiation (C_{SW}) and on longwave radiation (C_{LW}).

edges on the right part of Figure 3a) to derive the relative role of individual radiative feedbacks and forcing adjustments.

The increase in equilibrium temperature response is mainly attributable to the change in the total feedback parameter, even if the change in total forcing adjustment also contributes substantially. When looking at the decomposition by agents (middle part of Figure 3a), several agents are at play: both longwave and shortwave clouds contribute to the increase while water vapor and lapse rate changes contribute negatively to the change in equilibrium temperature. Note that the residual term is also relatively large. These results are confirmed when using other kernels to perform the decomposition (Table 6).

Table 6
Decomposition of the Difference in 4 × CO_2 Equilibrium Temperature Response Between AM5 and AM6 and the Sum of Contributions Derived From Each Intermediate Change in Atmospheric Configuration, for Each Radiative Kernel

	$\Delta_{ab}T_{eq}$	$\Delta_{ab}T_L$	$\Delta_{ab}T_{F_i^*} + \Delta_{ab}T_{\lambda_i}$						$\Delta_{ab}T_R$
			P	$L+W$	A	C_{SW}	C_{LW}	r	
Kernel					(K)				
					Total effect: AM6 minus AM5				
CM6	2.81	−0.07	0.00	−0.90	−0.27	0.96	2.17	1.09	−0.17
CM6-atm5	2.81	−0.07	-0.03	−0.81	−0.34	1.03	2.16	1.04	−0.17
CAM3	2.81	−0.07	0.00	−0.58	−0.15	0.85	2.28	0.65	−0.17
					Sum				
CM6	2.81	−0.07	0.12	−0.54	−0.17	−0.13	2.70	1.30	−0.40
CM6-atm5	2.81	−0.07	0.10	−0.47	−0.21	−0.08	2.70	1.24	−0.40
CAM3	2.81	−0.07	0.10	−0.30	−0.09	−0.21	2.87	0.91	−0.40

Note. The difference in equilibrium temperature response between model configurations a and b, $\Delta_{ab}T_{eq}$, is decomposed into the land warming adjustment contribution $\Delta_{ab}T_L$, into the individual radiative agents contribution $\Delta_{ab}T_{F_i^*} + \Delta_{ab}T_{\lambda_i}$ and the residual term $\Delta_{ab}T_R$ (see Equation 10). Radiative agents are the Planck feedback (P), the lapse rate and water vapor feedback ($L+W$), the albedo feedback (A), the cloud feedback on solar radiation (C_{SW}) and on longwave radiation (C_{LW}). See also Figure 3.

The climate sensitivity increase between AM5 and AM6 is primarily due to the net (longwave plus shortwave) cloud radiative responses. The differences in the SW and LW cloud feedbacks are similar ($\Delta_{ab}\lambda_{csw} = 0.25$ W. m^{-2}. K^{-1} and $\Delta_{ab}\lambda_{clw} = 0.23$ W.m^{-2}. K^{-1}), with a slightly larger contribution of the SW cloud feedback (see right part of Figure 3a). However, the total (forcing adjustment plus feedback) contribution of the LW component of the cloud change is equal to 2.17 K and is twice as large as the contribution of the SW cloud radiative response. This is due to both a negative contribution of the SW component of the cloud forcing adjustment and a positive contribution of the LW part of the forcing adjustment.

The linearized decomposition is compared to the DB08 decomposition (Figure 3b). This comparison illustrates the fact that this widely used decomposition (e.g., Vial et al., 2013) can lead to fallacious interpretation when quantifying the role of each feedback in climate sensitivity differences. In the case of the change in the equilibrium temperature response between AM5 and AM6 experiments, the DB08 decomposition minimizes the role of cloud change. In particular, it predicts that the water vapor plus lapse rate contribution is positive whereas it is negative with the linearized decomposition. In addition, the forcing change contribution is underestimated.

5.4. Contributions of Atmospheric Configuration Changes

The ECS decomposition used in previous section has been repeated for each model configuration change (Table 3) between AM5 and AM6 (Figure 5) and the sum of these configuration changes is shown in Figure 4b. Results from the change between AM5 and AM6 experiments (Figure 3a) are also shown in Figure 4a for reference. First, the comparison of the summed effects and of the direct effect calculation from AM5 to AM6 looks similar and confirms the leading role of the feedback parameter over the forcing adjustment and the important contribution of the cloud radiative responses. The LW component of the cloud contribution is well reproduced by the sum of the atmospheric configuration changes. However, for the contribution of the SW cloud change, the sum of individual model configurations does reflect a weak negative effect contrarily to the net positive effect found between AM5 and AM6. This mismatch is clear whatever kernel is used (Table 6). Thus, it cannot be attributed to the kernel in itself.

Looking at the individual configuration changes (Figure 5), the difference of equilibrium temperature response due to the change of the convection scheme ($\Delta_{con}T_{eq} = 3.04$ K) is substantially larger than the

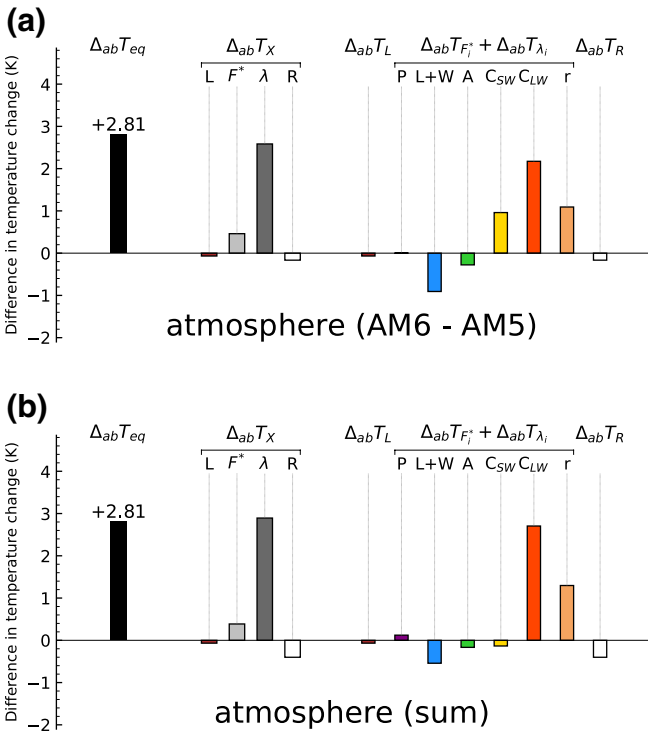

Figure 4. Decomposition of the difference in 4×CO_2 equilibrium temperature response between (a) AM5 and AM6 and (b) the sum of contributions derived from each intermediate change in atmospheric configuration (i.e., the sum of Figure 4 panels). In each panel, the difference in equilibrium temperature response between model configurations *a* and *b*, $\Delta_{ab}T_{eq}$ (black), is decomposed twice, first into the land warming adjustment contribution $\Delta_{ab}T_L$ (brown), the forcing adjustment contribution $\Delta_{ab}T_{F^*}$ (light gray), the feedback contribution $\Delta_{ab}T_\lambda$ (gray) and the residual term $\Delta_{ab}T_R$ (white), second (colored) into the individual radiative agents contribution $\Delta_{ab}T_{F_i^*} + \Delta_{ab}T_{\lambda_i}$, the land warming adjustment contribution $\Delta_{ab}T_L$ (brown) and the residual term $\Delta_{ab}T_R$ (white), $\Delta_{ab}T_{eq} = \Delta_{ab}T_L + \sum_i(\Delta_{ab}T_{F_i^*} + \Delta_{ab}T_{\lambda_i}) + \Delta_{ab}T_R$. Radiative agents are the Planck feedback (P), the lapse rate, and water vapor feedback (L + W), the albedo feedback (A), the cloud feedback on solar radiation (C_{SW}) and on longwave radiation (C_{LW}).

differences of ΔT_{eq} due to changes in vertical resolution, in cloud microphysics, in turbulence/cloud schemes or in cloud/aerosol optical properties. When looking at the decomposition by radiative agents, the sum of individual atmospheric configuration changes mimics the total contribution of LW cloud forcing adjustment and feedback changes (Figures 4 and S3). The dominant effect in total (forcing plus feedback) LW cloud contributions is the convection scheme change (Figures 5 and S4). This latter is also the predominant term in the summed contributions of the SW cloud forcing adjustment change (Figure S4). The modification of the convection scheme also pictures a large negative impact on the contribution of the SW cloud feedback. Changes in cloud optical properties, turbulence parameterization, cloud scheme, and cloud microphysics re-equilibrate the effect of the SW component of the cloud feedback (Figures 5 and S4). But the sum of individual configuration changes underestimates the (positive) total contribution (Figure 4). Note also that changing the vertical resolution and dynamics has led to a compensating effect on the forcing adjustment and feedback parameters. This effect is due to the contribution of the residual terms in the kernel decomposition (Figure S4).

Cloud feedback changes largely contributes to the climate sensitivity increase between AM5 and AM6 configurations. Zonal-mean values of the SW and LW cloud feedback changes (Figures 6a and 6b) offer another insight into the role of the individual configuration changes. The regional contributions of the cloud feedback changes are summarized in Figure 6c (see also Tables S6–S8). Results are shown for each individual configuration changes and for the tropical region (TROP; 30°S-30°N average), the Northern Hemisphere extratropical latitudes (eNH; 30°N-90°N average) and the Southern Hemisphere extratropical latitudes (eSH; 30°S-90°S average). Same conclusions can be drawn by looking at the changes of cloud contributions in equilibrium temperature response (not shown). The total SW cloud feedback change ($\Delta_{ab}\lambda_{csw} = 0.25$ W.m^{-2}. K^{-1}) is mainly due to both tropical regions (0.15 W.m^{-2}. K^{-1}) and southern extratropical regions (0.08 W.m^{-2}. K^{-1}). The increase in SW cloud feedback between AM5 and AM6 configuration is relatively homogeneous from 60°S to 30°N (Figure 6a). On the contrary, most of the increase in global-mean LW cloud feedback between AM5 and AM6 ($\Delta_{ab}\lambda_{csw} = 0.23$ W.m^{-2}. K^{-1}) is due to the tropical regions (Figure 6b).

Looking at the individual configuration changes, for the SW cloud feedback change, the moderate negative effect due to the tropical-mean change associated with the convection scheme change is counterbalanced by a sum of positive effects of the same order of magnitude (about 0.10 W.m^{-2}. K^{-1}) due to change in cloud optical properties, turbulence parameterization, cloud scheme, and cloud microphysics. Modification in microphysics, turbulence, or cloud scheme are not completely independent physical parameterizations. Because of this interplay between atmospheric parameterizations, conclusions drawn from the effect of changing a unique physical scheme must be considered with caution. The LW cloud feedback change is mainly due to an increase in tropical regions. More than 40% of the global-mean net cloud feedback increase is explained by the tropical-mean LW cloud feedback increase (0.20 W.m^{-2}. K^{-1}).

The convection scheme change pictures a large positive impact on the tropical LW cloud feedback change. Other parameterizations changes tend to counterbalance the convection scheme effect. The differences between the convection scheme used in CM5 model (Bougeault, 1985) and that used in CM6 model (Guérémy, 2011; Piriou et al., 2007) arise from many aspects. The cloud model used to estimate the vertical distribution of the convective quantities, including the entrainment and detrainment formulations,

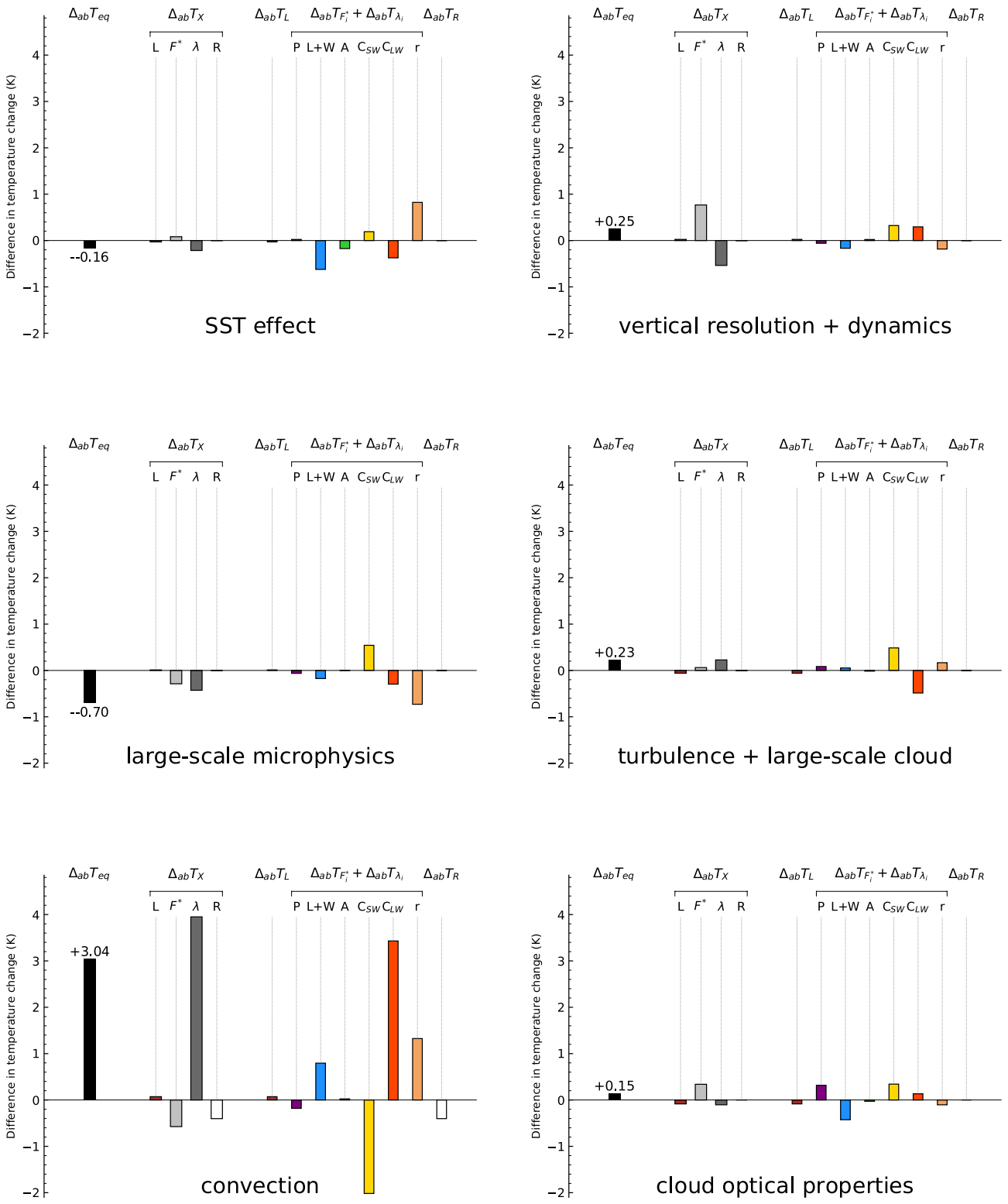

Figure 5. Same as Figure 3 for all intermediate atmospheric configuration changes listed in Table 3: AM5-s6 minus AM5 (SST effect), AM5-d6 minus AM5-s6 (vertical resolution + dynamics), AM5-m6 minus AM5-d6 (large-scale microphysics), AM5-t6 minus AM5-m6 (turbulence + large-scale cloud), AM5-c6 minus AM5-t6 (convection) AM6-AM5-c6 (cloud optical properties).

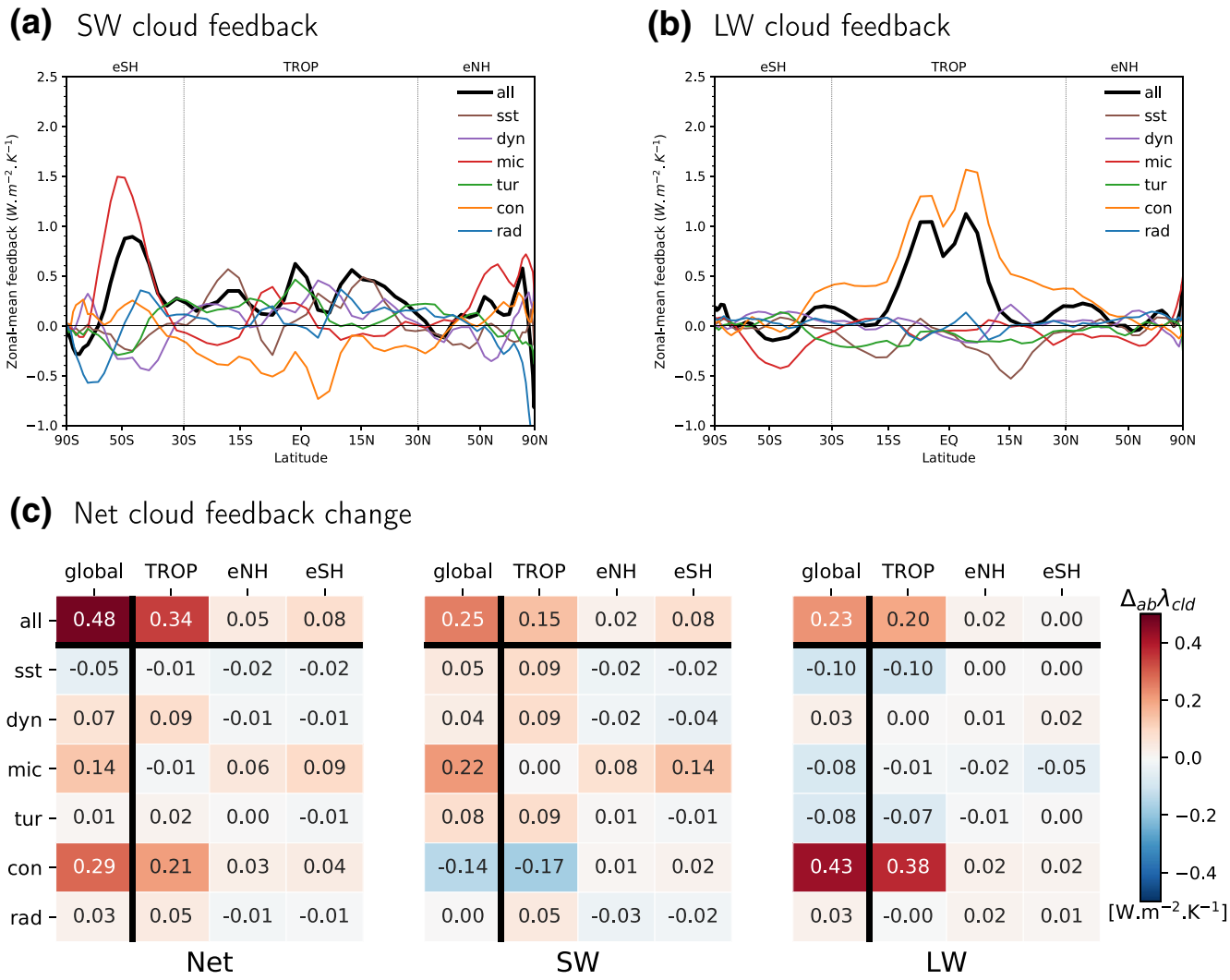

Figure 6. Zonal-mean (a) SW and (b) LW cloud feedback parameter changes for AM6 minus AM5 ("all," black lines) and for all intermediate atmospheric configuration changes listed in Table 3: AM5-s6 minus AM5 ("sst": SST effect), AM5-d6 minus AM5-s6 ("dyn": vertical resolution + dynamics), AM5-m6 minus AM5-d6 ("mic": large-scale microphysics), AM5-t6 minus AM5-m6 ("tur": turbulence + large-scale cloud), AM5-c6 minus AM5-t6 ("con": convection) AM6-AM5-c6 ("rad": cloud optical properties). Zonal-mean values are plotted against the sine of latitude. (c) Fractional contributions of regional mean terms to the total cloud feedback change. Colors indicate magnitude of the contributions which is also given by numbers in each cell. The tropical mean (TROP; 30°S-30°N average), the extratropical Northern Hemisphere mean (eNH; 30°N-90°N average) change and the extratropical Southern Hemisphere mean (eSH; 30°S-90°S average) change are multiplied by the fractional area of each region, so the global-mean change is the sum of the tropical-mean change, the extratropical Northern Hemisphere mean change and the extratropical Southern Hemisphere mean change.

the updraft vertical velocity equation, strongly differs between the two mass-flux schemes. Triggering and closure are based on a moisture flux convergence in the CM5 mass-flux scheme (Kuo, 1965) and on a dilute convective available potential energy (CAPE) relaxation in the CM6 convection scheme. Convective microphysical processes are treated in a very different way and strongly coupled to others components of the schemes. The lack of modularity of the corresponding numerical codes makes it difficult to clearly disentangle the role of each component of the scheme. However, some preliminary tests have been done and suggest that the treatment of the convective microphysics has a nonnegligible effect.

To go a step further, we investigate the change in upper-troposphere tropical cloud climatologies in the individual configuration changes. High-level cloud changes are the dominant contributor to LW cloud feedback at every latitude (e.g., Zelinka et al., 2012). First, the climatological mean of the tropical cloud fraction in the unperturbed states of AM5 and AM6 configurations (piSST_piCO$_2$ experiments) is plotted

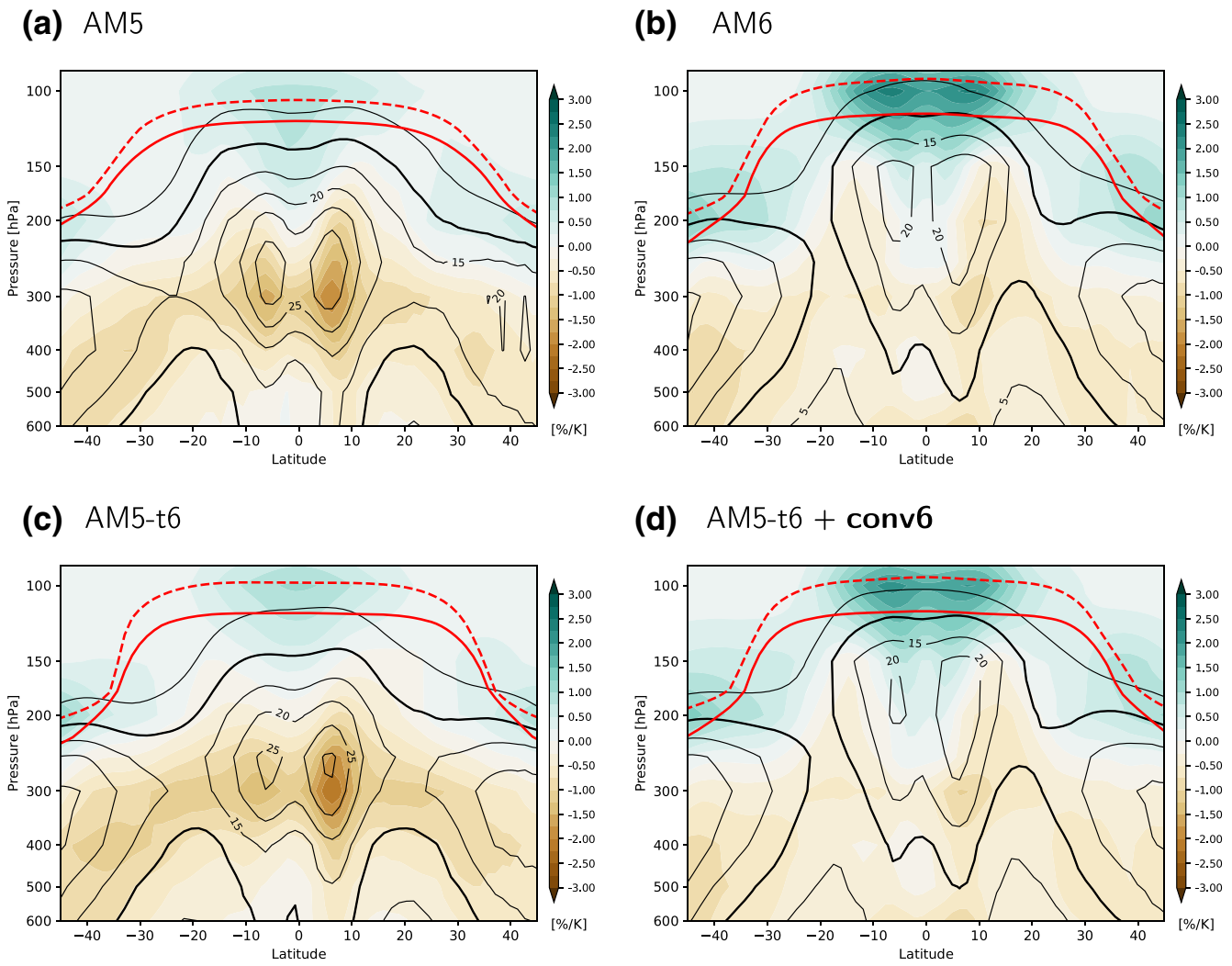

Figure 7. Zonal-mean cloud fraction climatologies (contours) and simulated changes (shading) for (a) AM5 configuration, (b) AM6 configuration, (c) AM5-t6 configuration, and (d) AM5-c6 configuration. The difference between AM-c6 and AM5-t6 only comes from a change in the convection scheme. Climatologies of cloud fraction (unit: %) are derived from piSST_piCO$_2$ experiments (line contour interval of 5%; thick line for 10% cloud fraction). Changes in cloud fraction (unit: %/K) are the difference between 4×SST_4×CO$_2$ and piSST_piCO$_2$ and are normalized by the tropical-mean (30°S-30°N) surface temperature change. The tropopause in piSST_piCO$_2$ (respectively 4×SST_4×CO$_2$) experiments is indicated with solid red line (resp. dashed red line). The height of the tropopause is determined from model temperature data using a standard definition (Reichler et al., 2003).

in Figures 7a and 7b. For both configurations, the tropical cloud fraction increases with altitude from 600 hPa to about 250-150 hPa and decreases above this height. However, the climatological cloud fraction peaks at about 250 hPa in AM5 and about 180 hPa in AM6. This difference in the altitude of the maximal climatological cloud fraction is the main difference between AM5 and AM6. The effect of convection scheme change is investigated through the comparison of AM5-t6 and AM5-c6 intermediate configurations. The difference between AM-c6 and AM5-t6 only comes from a change in the convection scheme. The localization of the maximal cloud fraction in AM5 is well reproduced by the AM5-t6 intermediate configuration. However, above this height, the tropical cloud fraction decreases more slowly in AM5 than in AM5-t6. The tropopause is also higher in AM5-t6. The change in the convection scheme has a large impact on the vertical profile of the climatological tropical cloud fraction. It leads to an increase of almost 10% at about 150 hPa. The convection scheme change seems to play an important role in driving this change in tropical high-level clouds.

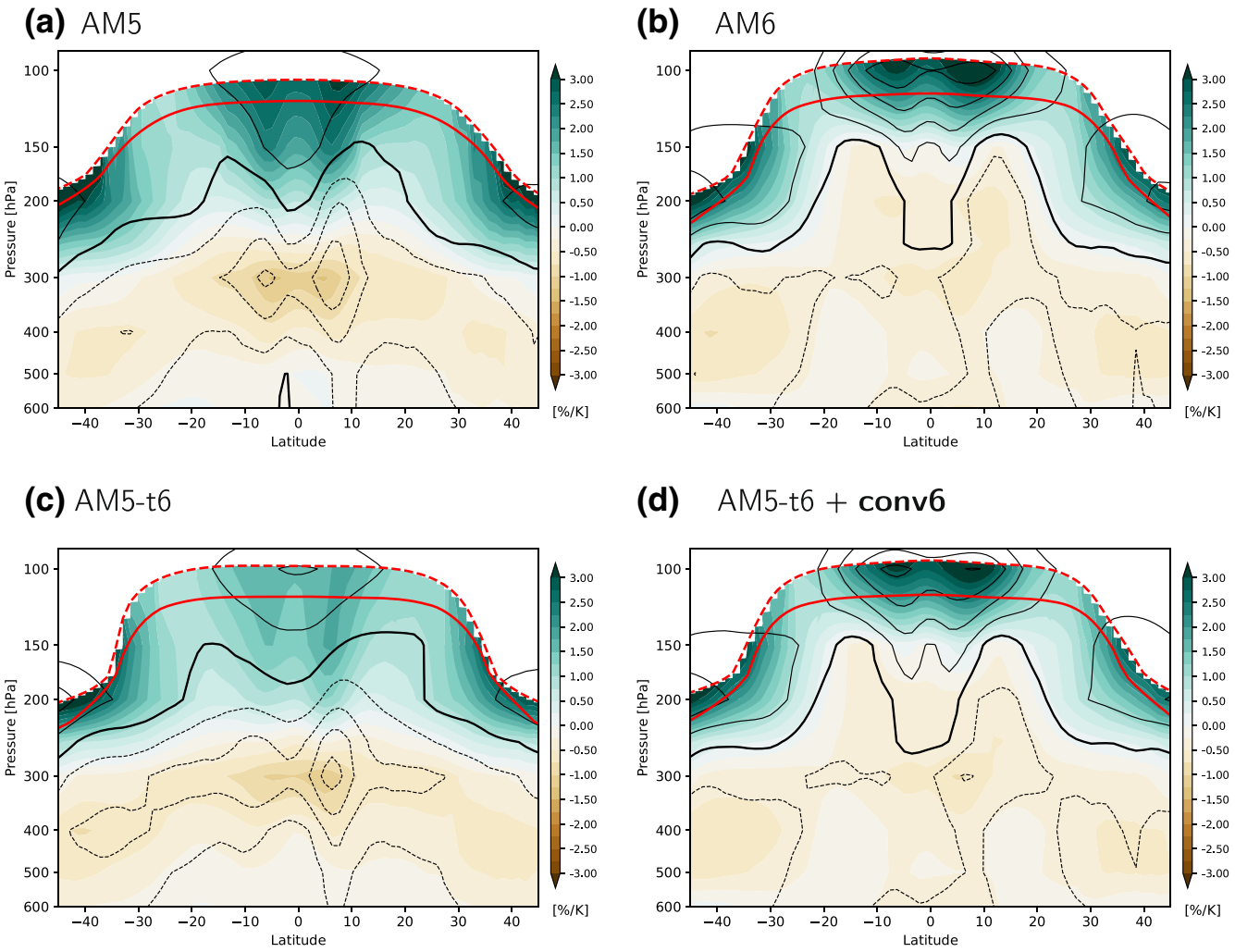

Figure 8. Zonal-mean simulated changes (contours) and predicted changes (shading) for (a) AM5 configuration, (b) AM6 configuration, (c) AM5-t6 configuration, and (d) AM5-c6 configuration. The simulated changes are identical to the changes shown in Figure 7 (line contour interval of 0.50%/K; thick zeroline). The predicted changes in cloud fraction (unit: %/K) are computed using the methodology described in Po-Chedley et al. (2019). The tropopause in piSST_piCO$_2$ (respectively 4×SST_4×CO$_2$) experiments is indicated with solid red line (resp. dashed red line). The area above the 4×SST_4×CO$_2$ tropopause is masked.

Moreover, the changes of cloud fraction in response to 4×CO$_2$ forcing (difference between 4×SST_4×CO$_2$ and piSST_piCO$_2$ experiments) are also shown in Figure 7 (shading). The responses are consistent with an upward shift of the climatological distribution of clouds with a decrease above the maximum and an increase near the tropopause. As for the climatological distribution, the change in convection scheme seems to be an important driver of the change in tropical high-level cloud fraction. Same conclusions can be drawn when looking at relative humidity changes (not shown).

As previously done in Po-Chedley et al. (2019), we use each configuration's climatology to estimate the expected change of cloud fraction by assuming that (i) cloud is an invariant function of temperature and (ii) the normalized profile of warming can be approximated by a dilute moist adiabatic (with $a = 0.5$ in Equation 7 of Romps [2016]). Using these two assumptions, the predicted change of cloud fraction is plotted in Figure 8. As in Po-Chedley et al. (2019) for the CMIP5 multimodel mean, the predicted change is consistent with the simulated change for each configuration. The vertical profile of the predicted change is well represented but the amplitude of the change is somewhat overestimated in particular for the AM5 and AM5-t6 configurations. Nevertheless, the larger increase in cloud fraction near the tropopause in AM6 is well predicted. This shows that the change in high-level cloud fraction in the equatorial region is related

to the climatological distribution of the thermodynamical and cloud profiles in the preindustrial climate. The convection scheme change seems to play an important role in driving these climatological profiles and hence the associated changes in tropical cloud radiative responses.

6. Conclusion

This study highlights the evolution of equilibrium temperature response to a quadrupling of atmospheric CO_2 concentration in the CNRM suite of climate models from version 5, CNRM-CM5.1 (6.5 K) to version 6, CNRM-CM6-1 (9.8 K) and its high-resolution counterpart, CNRM-CM6-1-HR (8.8 K). A particular attention is paid to the method used to decompose the equilibrium temperature response difference, by using fixed-SST/SIC experiments and a linear decomposition of the individual feedback diagnosed by a radiative kernel technique. The difference of $4\times CO_2$ equilibrium temperature response (about 1.0 K) between the standard and the high-resolution versions of CNRM-CM6 is not investigated in this study.

The traceability of this climate sensitivity change is first investigated using coupled ocean-atmosphere model climate change simulations. These simulations show that the increase in ECS is the result of changes in the atmospheric component. The increase in climate sensitivity between CNRM-CM5 version and CNRM-CM6 versions is a consequence of the numerous changes in the atmospheric component between the two versions. A series of experiments was carried out to assess what processes are responsible for the change in climate sensitivity.

The climate sensitivity increase is primarily due to the cloud radiative responses, with positive contributions of the longwave component (including both feedback and forcing adjustment) and of the shortwave feedback change. The contribution of the shortwave cloud forcing adjustment is negative. Tropical and extratropical regions contribute rather equally to the increase in SW cloud feedback whereas the LW cloud feedback mainly increases in the tropics. This LW tropical cloud feedback change seems to be due to a change in the climatology of high-level clouds. The convection scheme change appears to play an important role in driving the change in tropical climatological high clouds.

This work confirms the importance of cloud feedbacks in explaining the change of the ECS in recent climate models. Zelinka et al. (2020) shows that climate sensitivity is larger (on average) in CMIP6 than in CMIP5 due mostly to a stronger positive extratropical SW cloud feedback. The difference between CNRM-CM5 version and CNRM-CM6 versions shares some characteristics with the multimodel mean change. The increase of the shortwave cloud feedback contributes to the climate sensitivity increase in the CNRM climate models but contributions from tropical and extratropical regions are similar. The increase of the longwave cloud feedback is also an important contributor to the climate sensitivity increase. Moreover, the contribution of the shortwave cloud adjusted forcing is negative whereas the contribution of the longwave cloud forcing is positive, reinforcing the importance of the longwave part of the spectrum in the increase in climate sensitivity between CNRM-CM5 version and CNRM-CM6 versions. Concerning the reliability of the CNRM-CM versions, up to date, there is no reason to favor one version over the other. Reducing uncertainties in cloud feedbacks requires substantial efforts and several lines of research could be followed: process-oriented studies using large-eddy simulations, improving knowledge from recent field measurement campaigns and from global cloud resolving models.

Appendix A: Derivation of DB08 Decomposition

Following Equation 3, the equilibrium temperature response ΔT_{eq} writes:

$$\Delta T_{eq} = \Delta T_L - \frac{F^*_{tot}}{\lambda_{tot}}. \tag{A1}$$

By expanding $F^*_{tot} = \mathcal{F}_0 + \sum_i F^*_i$ and by denoting λ_P the Planck feedback parameter, we obtain:

$$\Delta T_{eq} = \Delta T_L - \frac{\mathcal{F}_0 + \sum_i F^*_i}{\lambda_P}\left(1 - \sum_{j\neq P}\frac{\lambda_j}{\lambda_{tot}}\right), \tag{A2}$$

and:

$$\Delta T_{eq} = \Delta T_L - \frac{\mathcal{F}_0}{\lambda_P} - \sum_i \frac{F_i^*}{\lambda_P} + \sum_{j \neq P} \frac{F_{tot}^*}{\lambda_P} \frac{\lambda_j}{\lambda_{tot}}. \tag{A3}$$

Finally, the DB08 decomposition writes:

$$\Delta T_{eq} = \Delta T_L + \sum_i \Delta T_{F_i^*} + \sum_j \Delta T_{\lambda_j}, \tag{A4}$$

with

$$\begin{aligned} \Delta T_{F_i^*} &= -F_i^* \,/\, \lambda_P \\ \Delta T_{\lambda_P} &= -\mathcal{F}_0 \,/\, \lambda_P \\ \Delta T_{\lambda_{j,j\neq P}} &= (F_{tot}^* \,/\, \lambda_P)(\lambda_j \,/\, \lambda_{tot}) \end{aligned} \tag{A5}$$

The DB08 decomposition of the change in the difference of the equilibrium temperature responses of two model configurations (denoted by a and b) writes:

$$\Delta_{ab} T_{eq} = \Delta_{ab} T_L + \sum_i \Delta_{ab} T_{F_i^*} + \sum_j \Delta_{ab} T_{\lambda_j} + \Delta_{ab} T_R, \tag{A6}$$

with

$$\begin{aligned} \Delta_{ab} T_L &= \Delta T_{L,b} - \Delta T_{L,a}, \\ \Delta_{ab} T_{F_i^*} &= -F_{i,b}^* \,/\, \lambda_{P,b} + F_{i,a}^* \,/\, \lambda_{P,a}, \\ \Delta_{ab} T_{\lambda_P} &= -\mathcal{F}_0 \,/\, \lambda_{P,b} + \mathcal{F}_0 \,/\, \lambda_{P,a}, \\ \Delta_{ab} T_{\lambda_{j,j\neq P}} &= (F_{tot,b}^* \,/\, \lambda_{P,b})(\lambda_{j,b} \,/\, \lambda_{tot,b}) - (F_{tot,a}^* \,/\, \lambda_{P,a})(\lambda_{j,a} \,/\, \lambda_{tot,a}), \\ \Delta_{ab} T_R &= 0. \end{aligned} \tag{A7}$$

Data Availability Statement

CMIP-6 CNRM-CM6-1 experiments are made available via the portal (https://esgf-node.llnl.gov/search/cmip6).

Acknowledgments
The authors would like to thank the entire CNRM-CM team for their support, in particular S. Sénési for his technical assistance.

References

Andrews, T., Gregory, J. M., & Webb, M. J. (2015). The dependence of radiative forcing and feedback on evolving patterns of surface temperature change in climate models. *Journal of Climate*, *28*(4), 1630–1648. https://doi.org/10.1175/JCLI-D-14-00545.1

Andrews, T., Gregory, J. M., Webb, M. J., & Taylor, K. E. (2012). Forcing, feedbacks and climate sensitivity in CMIP5 coupled atmosphere-ocean climate models. *Geophysical Research Letters*, *39*, L09712. https://doi.org/10.1029/2012GL051607

Block, K., & Mauritsen, T. (2013). Forcing and feedback in the MPI-ESM-LR coupled model under abruptly quadrupled CO_2: Forcing and feedback in the MPI-ESM-LR. *Journal of Advances in Modeling Earth Systems*, *5*(4), 676–691. https://doi.org/10.1002/jame.20041

Bodas-Salcedo, A., Mulcahy, J. P., Andrews, T., Williams, K. D., Ringer, M. A., Field, P. R., & Elsaesser, G. S. (2019). Strong dependence of atmospheric feedbacks on mixed-phase microphysics and aerosol-cloud interactions in HadGEM3. *Journal of Advances in Modeling Earth Systems*, *11*(6), 1735–1758. https://doi.org/10.1029/2019MS001688

Bony, S., Colman, R., Kattsov, V. M., Allan, R. P., Bretherton, C. S., Dufresne, J.-L., et al. (2006). How well do we understand and evaluate climate change feedback processes? *Journal of Climate*, *19*(15), 3445–3482. https://doi.org/10.1175/JCLI3819.1

Bony, S., & Dufresne, J.-L. (2005). Marine boundary layer clouds at the heart of tropical cloud feedback uncertainties in climate models. *Geophysical Research Letters*, *32*, L20806. https://doi.org/10.1029/2005GL023851

Bougeault, P. (1981). Modeling the trade-wind cumulus boundary-layer. Part I: Testing the ensemble cloud relations against numerical data. *Journal of Atmospheric Sciences*, *38*(11), 2414–2428. https://doi.org/10.1175/1520-0469(1981)038⟨2414:MTTWCB⟩2.0.CO;2

Bougeault, P. (1982). Cloud-ensemble relations based on the gamma probability distribution for the higher-order models of the Planetary Boundary Layer. *Journal of Atmospheric Science*, *39*, 2691–2700. https://doi.org/10.1175/1520-0469(1982)039⟨2691:CERBOT⟩2.0.CO;2

Bougeault, P. (1985). A simple parameterization of the large-scale effects of cumulus convection. *Monthly Weather Review*, *113*(12), 2108–2121. https://doi.org/10.1175/1520-0493

Bougeault, P., & Lacarrère, P. (1989). Parameterization of orography-induced turbulence in a mesobeta-scale model. *Monthly Weather Review*, *117*, 1872–1890. https://doi.org/10.1175/1520-0493

Caldwell, P. M., Zelinka, M. D., Taylor, K. E., & Marvel, K. (2016). Quantifying the sources of intermodel spread in equilibrium climate sensitivity. *Journal of Climate*, *29*(2), 513–524. https://doi.org/10.1175/JCLI-D-15-0352.1

Cess, R. D., Potter, G. L., Blanchet, J. P., Boer, G. J., Del Genio, A. D., Déqué, M., et al. (1990). Intercomparison and interpretation of climate feedback processes in 19 atmospheric general circulation models. *Journal of Geophysical Research*, *95*(D10), 16601. https://doi.org/10.1029/JD095iD10p16601

Cheng, Y., Canuto, V. M., & Howard, A. M. (2002). An improved model for the turbulent PBL. *Journal of Atmospheric Science*, *59*, 1550–1565. https://doi.org/10.1175/1520-0469(2002)059⟨1550:AIMFTT⟩2.0.CO;2

Collins, M., Booth, B. B. B., Bhaskaran, B., Harris, G. R., Murphy, J. M., Sexton, D. M. H., & Webb, M. J. (2010). Climate model errors, feedbacks and forcings: A comparison of perturbed physics and multi-model ensembles. *Climate Dynamics*, *36*(9–10), 1737–1766. https://doi.org/10.1007/s00382-010-0808-0

Craig, A., Valcke, S., & Coquart, L. (2017). Development and performance of a new version of the OASIS coupler, OASIS3-MCT_3.0. *Geoscientific Model Development*, *10*(9), 3297–3308. https://doi.org/10.5194/gmd-10-3297-2017

Cuxart, J., Bougeault, P., & Redelsperger, J.-L. (2000). A turbulence scheme allowing for mesoscale and large-eddy simulations. *Quarterly Journal of the Royal Meteorological Society*, *126*(562), 1–30. https://doi.org/10.1002/qj.49712656202

de Lavergne, C., Madec, G., Le Sommer, J., Nurser, A. J. G., & Naveira Garabato, A. C. (2015). The impact of a variable mixing efficiency on the abyssal overturning. *Journal of Physical Oceanography*, *46*(2), 663–681. https://doi.org/10.1175/JPO-D-14-0259.1

Decharme, B., Delire, C., Minvielle, M., Colin, J., Vergnes, J.-P., Alias, A., et al. (2019). Recent changes in the ISBA-CTRIP land surface system for use in the CNRM-CM6 climate model and in global off-line hydrological applications. *Journal of Advances in Modeling Earth Systems*, *11*, 207–1252. https://doi.org/10.1029/2018MS001545

Dufresne, J.-L., & Bony, S. (2008). An assessment of the primary sources of spread of global warming estimates from coupled atmosphere-ocean models. *Journal of Climate*, *21*(19), 5135–5144. https://doi.org/10.1175/2008JCLI2239.1

Ebert, E. E., & Curry, J. A. (1992). A parameterization of ice cloud optical properties for climate models. *Journal of Geophysical Research*, *97*(D4), 3831. https://doi.org/10.1029/91JD02472

Etminan, M., Myhre, G., Highwood, E. J., & Shine, K. P. (2016). Radiative forcing of carbon dioxide, methane, and nitrous oxide: A significant revision of the methane radiative forcing. *Geophysical Research Letters*, *43*, 12614–12623. https://doi.org/10.1002/2016GL071930

Eyring, V., Bony, S., Meehl, G. A., Senior, C. A., Stevens, B., Stouffer, R. J., & Taylor, K. E. (2016). Overview of the Coupled Model Intercomparison Project phase 6 (CMIP6) experimental design and organization. *Geoscientific Model Development*, *9*(5), 1937–1958. https://doi.org/10.5194/gmd-9-1937-2016

Flato, G., Marotzke, J., Abiodun, B., Braconnot, P., Chou, S. C., Collins, W., et al. (2013). *Evaluation of Climate models. Climate Change 2013: The physical science basis.* Contribution of Working Group I to the Fifth Assessment Report of the Intergovernmental panel on Climate Change. Cambridge, UK and New York, NY: Cambridge University Press.

Fu, Q. (1996). An accurate parameterization of the solar radiative properties of cirrus clouds for climate models. *Journal of Climate*, *9*(9), 2058–2082. https://doi.org/10.1175/1520-0442

Gent, P. R., & McWilliams, J. C. (1990). Isopycnal mixing in ocean circulation models. *Journal of Physical Oceanography*, *20*, 150–155. https://doi.org/10.1175/1520-0485(1990)020⟨0150:IMIOCM⟩2.0.CO;2

Geoffroy, O., & Saint-Martin, D. (2020). Equilibrium- and transient-state dependencies of climate sensitivity: Are they important for climate projections? *Journal of Climate*, *33*(5), 1863–1879. https://doi.org/10.1175/JCLI-D-19-0248.1

Geoffroy, O., Saint-Martin, D., & Ribes, A. (2012). Quantifying the sources of spread in climate change experiments. *Geophysical Research Letters*, *39*, L24703. https://doi.org/10.1029/2012GL054172

Geoffroy, O., Saint-Martin, D., Voldoire, A., Salas y Mélia, D., & Sénési, S. (2014). Adjusted radiative forcing and global radiative feedbacks in CNRM-CM5, a closure of the partial decomposition. *Climate Dynamics*, *42*(7–8), 1807–1818. https://doi.org/10.1007/s00382-013-1741-9

Geoffroy, O., Sherwood, S. C., & Fuchs, D. (2017). On the role of the stratiform cloud scheme in the inter-model spread of cloud feedback. *Journal of Advances in Modeling Earth Systems*, *9*, 423–437. https://doi.org/10.1002/2016MS000846

Gettelman, A., Hannay, C., Bacmeister, J. T., Neale, R. B., Pendergrass, A. G., Danabasoglu, G., et al. (2019). High climate sensitivity in the Community Earth System Model version 2 (CESM2). *Geophysical Research Letters*, *46*(14), 8329–8337. https://doi.org/10.1029/2019GL083978

Gettelman, A., Kay, J. E., & Shell, K. M. (2012). The evolution of climate sensitivity and climate feedbacks in the Community Atmosphere Model. *Journal of Climate*, *25*(5), 1453–1469. https://doi.org/10.1175/JCLI-D-11-00197.1

Gregory, J. M., Andrews, T., & Good, P. (2015). The inconstancy of the transient climate response parameter under increasing CO_2. *Philosophical Transactions of the Royal Society A: Mathematical, Physical and Engineering Sciences*, *373*, 20140417. https://doi.org/10.1098/rsta.2014.0417

Gregory, J. M., Ingram, W. J., Palmer, M. A., Jones, G. S., Stott, P. A., Thorpe, R. B., et al. (2004). A new method for diagnosing radiative forcing and climate sensitivity. *Geophysical Research Letters*, *31*, L03205. https://doi.org/10.1029/2003GL018747

Gregory, J., & Webb, M. (2008). Tropospheric adjustment induces a cloud component in CO_2 forcing. *Journal of Climate*, *21*(1), 58–71. https://doi.org/10.1175/2007JCLI1834.1

Guérémy, J.-F. (2011). A continuous buoyancy based convection scheme: One-and three-dimensional validation. *Tellus A: Dynamic Meteorology and Oceanography*, *63*(4), 687–706. https://doi.org/10.1111/j.1600-0870.2011.00521.x

Hansen, J., Lacis, A., Rind, D., Russell, G., Stone, P., Fung, I., et al. (1984). Climate sensitivity: Analysis of feedback mechanisms. In J. E. Hansen & T. Takahashi (Eds.), Geophysical Monograph Series (Vol. 29, pp. 130–163). Washington, DC: American Geophysical Union. https://doi.org/10.1029/GM029p0130

Keenan, T. F., Hollinger, D. Y., Bohrer, G., Dragoni, D., Munger, J. W., Schmid, H. P., & Richardson, A. D. (2013). Increase in forest water-use efficiency as atmospheric carbon dioxide concentrations rise. *Nature*, *499*(7458), 324–327. https://doi.org/10.1038/nature12291

Kessler, E. (1969). On distribution and continuity of water substance in atmospheric circulations. *Meteorological Monographs*, *10*(32), 88. https://doi.org/10.1007/978-1-935704-36-2_1

Kuo, H. L. (1965). On formation and Intensification of tropical cyclones through latent heat release by cumulus convection. *Journal of Atmospheric Science*, *22*, 40–63. https://doi.org/10.1175/1520-0469(1965)022<0040:OFAIOT>2.0.CO;2

Lopez, P. (2002). Implementation and validation of a new prognostic large-scale cloud and precipitation scheme for climate and data-assimilation purposes. *Quarterly Journal of the Royal Meteorological Society*, *128*(579), 229–257. https://doi.org/10.1256/00359000260498879

Madec, G., Bourdalé-Badie, R., Bouttier, P.-A., Bricaud, C., Bruciaferri, D., Calvert, D., et al. (2017). NEMO ocean engine. *Zenodo*. https://doi.org/10.5281/ZENODO.1472492

Medeiros, B., Stevens, B., Held, I. M., Zhao, M., Williamson, D. L., Olson, J. G., & Bretherton, C. S. (2008). Aquaplanets, climate sensitivity, and low clouds. *Journal of Climate*, *21*, 4974–4991. https://doi.org/10.1175/2008JCLI1995.1

Meehl, G. A., Stocker, T. F., Collins, W. D., Friedlingstein, P., Gaye, A. T., Gregory, J. M., et al. (2007). *Global Climate Projections. Climate Change 2007: The scientific basis*. Cambridge, UK: Cambridge University Press.

Mellor, G. L., & Yamada, T. (1982). Development of a turbulence closure model for geophysical fluid problems. *Reviews of Geophysics*, *20*(4), 851–875. https://doi.org/10.1029/RG020i004p00851

Piriou, J.-M., Redelsperger, J.-L., Geleyn, J.-F., Lafore, J.-P., & Guichard, F. (2007). An approach for convective parameterization with memory: Separating microphysics and transport in grid-scale equations. *Journal of the Atmospheric Sciences*, *64*(11), 4127–4139. https://doi.org/10.1175/2007JAS2144.1

Po-Chedley, S., Zelinka, M. D., Jeevanjee, N., Thorsen, T. J., & Santer, B. D. (2019). Climatology explains intermodel spread in tropical upper tropospheric cloud and relative humidity response to greenhouse warming. *Geophysical Research Letters*, *46*(22), 13399–13409. https://doi.org/10.1029/2019GL084786

Qu, X., Hall, A., Klein, S. A., & Caldwell, P. M. (2014). On the spread of changes in marine low cloud cover in climate model simulations of the 21st century. *Climate Dynamics*, *42*(9–10), 2603–2626. https://doi.org/10.1007/s00382-013-1945-z

Reichler, T., Dameris, M., & Sausen, R. (2003). Determining the tropopause height from gridded data. *Geophysical Research Letters*, *30*, 2042. https://doi.org/10.1029/2003GL018240

Ricard, J. L., & Royer, J. F. (1993). A statistical cloud scheme for use in an AGCM. *Annales Geophysicae*, *11*, 1095–1115

Ringer, M. A., Andrews, T., & Webb, M. J. (2014). Global-mean radiative feedbacks and forcing in atmosphere-only and coupled atmosphere-ocean climate change experiments. *Geophysical Research Letters*, *41*(11), 4035–4042. https://doi.org/10.1002/2014GL060347

Romps, D. M. (2016). Clausius–Clapeyron scaling of CAPE from analytical solutions to RCE. *Journal of the Atmospheric Sciences*, *73*(9), 3719–3737. https://doi.org/10.1175/JAS-D-15-0327.1

Shell, K. M., Kiehl, J. T., & Shields, C. A. (2008). Using the radiative kernel technique to calculate climate feedbacks in NCAR's Community Atmospheric Model. *Journal of Climate*, *21*(10), 2269–2282. https://doi.org/10.1175/2007JCLI2044.1

Sherwood, S. C., Bony, S., & Dufresne, J.-L. (2014). Spread in model climate sensitivity traced to atmospheric convective mixing. *Nature*, *505*(7481), 37–42. https://doi.org/10.1038/nature12829

Simmons, H. L., Jayne, S. R., Laurent, L. C. S., & Weaver, A. J. (2004). Tidally driven mixing in a numerical model of the ocean general circulation. *Ocean Modelling*, *6*(3), 245–263. https://doi.org/10.1016/S1463-5003(03)00011-8

Slingo, A. (1988). A GCM parameterization for the shortwave radiative properties of water clouds. *Journal of Atmospheric Sciences*, *46*(10), 1419–1427. https://doi.org/10.1175/1520-0469(1989)046<1419:AGPFTS>2.0.CO;2

Smith, R. N. (1990). A scheme for predicting layer clouds and their water content in a general circulation model. *Quarterly Journal of the Royal Meteorological Society*, *116*(492), 435–460. https://doi.org/10.1002/qj.49711649210

Smith, E. A., & Shi, L. (1992). Surface forcing of the infrared cooling profile over the Tibetan plateau. Part I: Influence of relative longwave radiative heating at high altitude. *Journal of Atmospheric Science*, *49*, 805–822. https://doi.org/10.1175/1520-0469(1992)049⟨0805:SFOTIC⟩2.0.CO;2

Soden, B. J., & Held, I. M. (2006). An assessment of climate feedbacks in coupled ocean-atmosphere models. *Journal of Climate*, *19*(14), 3354–3360. https://doi.org/10.1175/JCLI3799.1

Soden, B. J., Held, I. M., Colman, R., Shell, K. M., Kiehl, J. T., & Shields, C. A. (2008). Quantifying climate feedbacks using radiative kernels. *Journal of Climate*, *21*(14), 3504–3520. https://doi.org/10.1175/2007JCLI2110.1

Tan, I., Storelvmo, T., & Zelinka, M. D. (2016). Observational constraints on mixed-phase clouds imply higher climate sensitivity. *Science*, *352*(6282), 224–227. https://doi.org/10.1126/science.aad5300

Taylor, K. E., Stouffer, R. J., & Meehl, G. A. (2012). An overview of CMIP5 and the experiment design. *Bulletin of the American Meteorological Society*, *93*(4), 485–498. https://doi.org/10.1175/BAMS-D-11-00094.1

Tomassini, L., Geoffroy, O., Dufresne, J.-L., Idelkadi, A., Cagnazzo, C., Block, K., et al. (2013). The respective roles of surface temperature driven feedbacks and tropospheric adjustment to CO_2 in CMIP5 transient climate simulations. *Climate Dynamics*, *41*(11–12), 3103–3126. https://doi.org/10.1007/s00382-013-1682-3

Tomassini, L., Voigt, A., & Stevens, B. (2015). On the connection between tropical circulation, convective mixing, and climate sensitivity: On tropical circulation, convective mixing, and climate sensitivity. *Quarterly Journal of the Royal Meteorological Society*, *141*(689), 1404–1416. https://doi.org/10.1002/qj.2450

Vial, J., Dufresne, J.-L., & Bony, S. (2013). On the interpretation of inter-model spread in CMIP5 climate sensitivity estimates. *Climate Dynamics*, *41*(11–12), 3339–3362. https://doi.org/10.1007/s00382-013-1725-9

Voldoire, A., Saint-Martin, D., Sénési, S., Decharme, B., Alias, A., Chevallier, M., et al. (2019). Evaluation of CMIP6 DECK experiments with CNRM-CM6-1. *Journal of Advances in Modeling Earth Systems*, *11*, 2177–2213. https://doi.org/10.1029/2019MS001683

Voldoire, A., Sanchez-Gomez, E., Salas y Mélia, D., Decharme, B., Cassou, C., Sénési, S., et al. (2013). The CNRM-CM5.1 global climate model: Description and basic evaluation. *Climate Dynamics*, *40*(9–10), 2091–2121. https://doi.org/10.1007/s00382-011-1259-y

Wetherald, R. T., & Manabe, S. (1988). Cloud feedback processes in a general circulation model. *Journal of Atmospheric Science*, *45*, 1397–1416. https://doi.org/10.1175/1520-0469(1988)045⟨1397:CFPIAG⟩2.0.CO;2

Winton, M., Takahashi, K., & Held, I. M. (2010). Importance of ocean heat uptake efficacy to transient climate change. *Journal of Climate*, *23*(9), 2333–2344. https://doi.org/10.1175/2009JCLI3139.1

Zelinka, M. D., Klein, S. A., & Hartmann, D. L. (2012). Computing and partitioning cloud feedbacks using cloud property histograms. Part I: Cloud radiative kernels. *Journal of Climate*, *25*(11), 3715–3735. https://doi.org/10.1175/JCLI-D-11-00248.1

Zelinka, M. D., Klein, S. A., Taylor, K. E., Andrews, T., Webb, M. J., Gregory, J. M., & Forster, P. M. (2013). Contributions of different cloud types to feedbacks and rapid adjustments in CMIP5*. *Journal of Climate*, *26*(14), 5007–5027. https://doi.org/10.1175/JCLI-D-12-00555.1

Zelinka, M. D., Myers, T. A., McCoy, D. T., Po-Chedley, S., Caldwell, P. M., Ceppi, P., et al. (2020). Causes of higher climate sensitivity in CMIP6 models. *Geophysical Research Letters*, *47*, e2019GL085782. https://doi.org/10.1029/2019GL085782

Zhao, M., Golaz, J.-C., Held, I. M., Ramaswamy, V., Lin, S.-J., Ming, Y., et al. (2016). Uncertainty in model climate sensitivity traced to representations of cumulus precipitation microphysics. *Journal of Climate*, *29*(2), 543–560. https://doi.org/10.1175/JCLI-D-15-0191.1